Journal of The
Electrochemical Society

OPEN ACCESS

DFT Study of Cl$^-$ Ingress into Organic Self-Assembled Monolayers on Aluminum

To cite this article: Fatah Chiter *et al* 2023 *J. Electrochem. Soc.* **170** 071504

View the article online for updates and enhancements.

You may also like

- The Effect of Climate Change on some Agricultural Crop Production in Basrah Governorate
  Bilal Hussein Mahood Al-Hussein, Kadhim Abdul Wahhab Al-Asadi and Widad M. Taher Al-Asadi
- Enhanced Oxygen Reduction Activity on Silver-Palladium Alloyed Thin Film Electrocatalysts in Alkaline Media
  Jose Andres Zamora Zeledon, Michaela Burke Stevens, G.T. Kasun Kalhara Gunasooriya et al.
- The activities and funding of IRPA: an overview
  Geoffrey Webb

PAT-Tester-x-8 Potentiostat:
Modular Solution for Electrochemical Testing!

EL-CELL®
electrochemical test equipment

✓ Flexible Setup with up to 8 Independent Test Channels!
Each with a fully equipped Potentiostat, Galvanostat and EIS!

✓ Perfect Choice for Small-Scale and Special Purpose Testing!
Suited for all 3-electrode, optical, dilatometry or force test cells from EL-CELL.

✓ Complete Solution with Extensive Software!
Plan, conduct and analyze experiments with EL-Software.

✓ Small Footprint, Easy to Setup and Operate!
Usable inside a glove box. Full multi-user, multi-device control via LAN.

Scan me!

Contact us:
☎ +49 40 79012-734
✉ sales@el-cell.com
🌐 www.el-cell.com

This content was downloaded from IP address 193.2.7.100 on 29/04/2025 at 09:02

Journal of The Electrochemical Society, 2023 **170** 071504

DFT Study of Cl^- Ingress into Organic Self-Assembled Monolayers on Aluminum

Fatah Chiter,[1] Dominique Costa,[1,z] Matic Poberžnik,[2] Ingrid Milošev,[2]
Philippe Marcus,[1] and Anton Kokalj[2,z]

[1] *PSL Research University, CNRS - Chimie ParisTech, Institut de Recherche de Chimie Paris (IRCP), Physical Chemistry of Surfaces Group, 75005 Paris, France*
[2] *Department of Physical and Organic Chemistry, Jožef Stefan Institute, Jamova 39, SI-1000 Ljubljana, Slovenia*

We address the mechanism by which organic layers on aluminum substrate hinder the penetration of Cl^- toward the metal substrate. Localized corrosion by chlorides on Al and its alloys is a major problem, and organic molecules that form self-assembled monolayers on metal substrates may provide efficient corrosion protection. In one of our previous works, we established experimentally that long-chain *n*-alkyl carboxylic acids form protective layers against Cl^- corrosion on Al substrates. In a different work, we identified, using implicit models of the organic layer and metal substrate, two essential effects by which organic layers hinder the penetration of Cl^- ions toward the metal substrate. The first effect is due to the inferior solvation of ions in the organic layer compared to that in an aqueous solvent. The second effect is due to the electric field at the electrochemical interface, and the extent to which it affects the penetration of Cl^- depends on the electrode potential and the thickness of the organic layer. Both effects are related to a low dielectric constant of the self-assembled monolayer. In the present study, we continue our investigation and explicitly model the organic monolayer and Al substrate using density-functional-theory calculations. To this end, we consider organic monolayers consisting of either dodecanoic- or hexanoic-acid molecules. Current calculations confirm the findings of the simplified implicit models, i.e. the energy barrier for the Cl^- penetration increases with the thickness of the organic monolayer and with Cl^- concentration in the monolayer. Furthermore, we propose a new mechanism by which Cl^- penetrates the organic monolayer. Due to the considerably inferior solvation of Cl^- in the organic layer compared to that in water, calculations suggest that it is energetically easier to locally "open" the organic monolayer by creating a hole large enough to accommodate water molecules and Cl^-. The presence of water molecules ensures a stronger Cl^- solvation and a better electrostatic screening between anions. While the energy barrier for the Cl^- penetration via the local "opening" mechanism is suggested to be smaller than for the penetration of Cl^- into dense homogeneous organic monolayer, it is still significant enough to pose a considerable kinetic barrier for the penetration of Cl^- from the aqueous solution into the organic monolayer at room temperature.

[DOI: 10.1149/1945-7111/ace334]

Manuscript submitted February 22, 2023; revised manuscript received June 27, 2023. Published July 14, 2023. *This paper is part of the JES Focus Issue on Critical Factors in Localized Corrosion in Honor of Gerald Frankel.*

Under ambient conditions, an aluminum surface is covered with a thin/ultrathin oxide film, which protects it against corrosion. However, we demonstrated that an ultrathin oxide film (5 Å thick) is not protective against the cathodic reaction,[1] which can in principle be mitigated by the use of appropriate corrosion inhibitors. In our subsequent works, we have shown with computational studies based on density-functional theory (DFT) that gallic acid, silanes, and linear carboxylic acids (CAs) can adsorb on oxidized Al surfaces.[2–5] The –COOH anchor group of CAs was investigated for its ability to interact with aluminum substrates and form chemical bonds and H-bonds with a surface. We also performed joint experimental and computational studies of the adsorption of linear CAs, $C_nH_{2n}O_2$ (labeled as CA-*n*), with different chain lengths.[5–7] We demonstrated that CA-12 and larger molecules are protective against pitting by Cl^- ions. The adsorption of a full layer of organic molecules, hereinafter referred to as the self-assembled monolayer (SAM), was evidenced by XPS and ToF-SIMS in the case of CA-12.[6] The experimental results are coherent with a coverage of about 4.7 molecules/nm^2, as calculated with DFT.

We have also performed a systematic DFT study of *n*-alkyl CAs adsorption of different alkyl chain lengths on two models of the oxidized Al surface.[5] This computational study confirmed that the magnitude of the adsorption free energy increases with increasing alkyl chain length, indicating that SAM formation is more favored for molecules containing longer alkyl chains. In the SAM, CAs molecules are tilted by about 40° ± 10° from the surface normal to optimize the lateral cohesive intermolecular interactions. Due to this tilt, the effective coverage of the surface increases with the chain length (Fig. 1). Note that the maximum monolayer coverage is given by the interplay of the steric footprint of the carboxylic head group and the surface site distribution. Due to the mismatch between the two, upright CAs neither completely cover the surface at maximum monolayer coverage nor make the lateral intermolecular interactions optimal (Fig. 1). Tilted alkyl chains, therefore, cover the surface more effectively. Furthermore, longer tilted alkyl chains display—due to increased lateral cohesive forces—a more exergonic adsorption free energy and a more organized SAM structure, resulting in a more stable and protective molecular film on the surface. In contrast, upright alkyl chains should be much less protective because too long distances between the chains make the SAM structure "open", and solvent molecules and Cl^- ions can penetrate the SAM much more easily (Fig. 1).

We thus hypothesized that SAMs consisting of long-chain tilted CA molecules might effectively hinder the penetration of Cl^- toward the Al substrate[5,6] and, consequently, protect it against Cl^- pitting because it is well established that the first step in Cl^- pitting is associated with chloride adsorption and either thinning of the passive film[8] or chloride diffusion into the passive layer.[9] From a kinetic point of view, this implies that SAM should pose a substantial energy barrier to the diffusion of Cl^- from the aqueous solvent toward the Al substrate. To make this hypothesis stronger, in a previous paper[10] some of us investigated by what mechanism SAMs inhibit the penetration of chlorides toward the metal substrate, by utilizing a simplified computational model. In this model, the Al substrate, the organic SAM film, and the aqueous solvent were described implicitly as dielectric continuum slabs, whereas Cl^- ions and Na^+ counterions were treated explicitly by DFT. This model is called herein the semi-implicit model ("semi" because ions were treated explicitly, and "implicit" because the surface and bulk phases

---

[z] E-mail: dominique.costa@chimieparistech.psl.eu; tone.kokalj@ijs.si

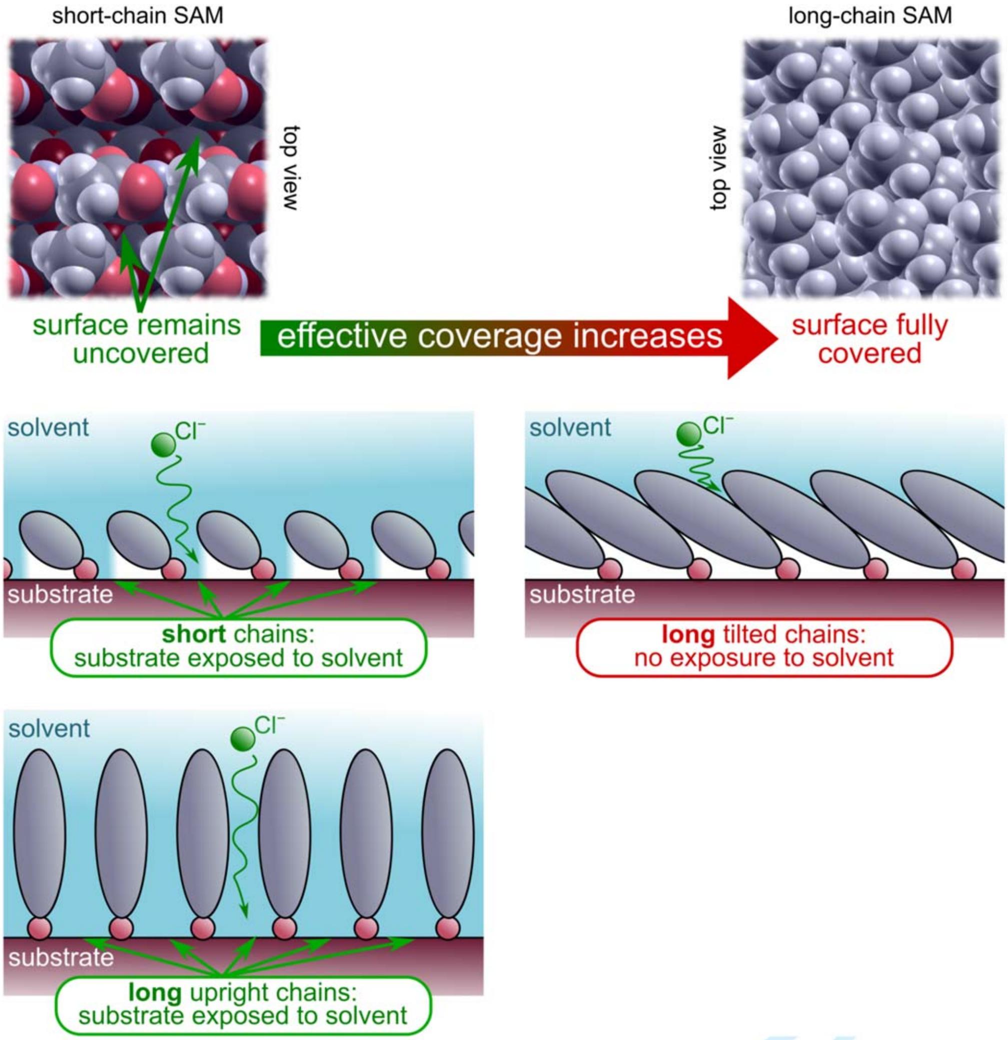

Figure 1. A schematic illustration that the effective surface coverage increases with the length of the alkyl chain of tilted CA molecules. The maximum monolayer coverage is given by the interplay of the steric footprint of the carboxylic head group and the surface site distribution. Due to the mismatch between the two, neither the short-chain nor the perpendicular long-chain CA molecules fully cover the surface, leaving the Al substrate potentially exposed to solvent. This suggests a much easier penetration of Cl^- from the aqueous solution toward the Al substrate. Atoms in the top-row snapshots are plotted with van der Waals radii.

were treated implicitly) and is labeled as implicit-SAM. We identified two essential effects by which SAMs hinder the penetration of Cl^- ions toward the metal substrate. The first is due to considerably inferior solvation of ions in the organic layer (a SAM film can be seen as a smectic liquid) compared to that in an aqueous solvent. The second effect is due to the electric field at the electrochemical interface, and the extent to which it affects the penetration of Cl^- depends on the electrode potential and the thickness of the organic layer. Other effects, such as local deformation of the organic layer during Cl^- penetration and inhomogeneities in the SAM film, could not be described by the simplified semi-implicit model and are considered herein using DFT-based models, where the Al substrate, the SAM film, and ions are treated explicitly and only the aqueous solvent implicitly. We will refer to these models as the semi-explicit DFT models ("semi" because the aqueous solvent is treated implicitly and "explicit" because all other components are treated explicitly).

The purpose of the current paper is, therefore, to study the penetration of Cl^- ions from an aqueous solvent into SAM toward the Al substrate using the semi-explicit DFT-based models. However, modeling charged "objects" is problematic when periodic-boundary conditions (PBC) are used and should be exercised carefully to avoid electrostatic artifacts. This issue was thoroughly investigated in the previous paper.[10] The usual approach is to add counterions into a supercell to achieve charge neutrality. However, this does not eliminate electrostatic artifacts, particularly when 3D PBC are used, which are typical of plane-wave DFT codes. A simple, though computationally inefficient, way to eliminate 3D PBC artifacts is to use a symmetric setup, where the water/SAM/substrate system is modeled by a double-sided water/SAM/substrate \SAM\water model. In such a model, ions are symmetrically added above and below the substrate so that the dipole created by ions on one side of the substrate is canceled by the counter-dipole created on the other side of the substrate.

However, even when 3D PBC artifacts are appropriately dealt with, the effects of 2D PBC remain. Due to 2D PBC, Cl^- ions and counterions (e.g., Na^+) form two layers of charges reminiscent of a parallel plate capacitor (Fig. 2a). As the Cl^- ion moves in the simulation away from the Na^+ ion toward the substrate, the whole infinite Cl^- layer moves. Because the electrostatic potential in the parallel plate capacitor is linear, the potential energy raises linearly with increasing the Na–Cl distance, provided that Cl^- is far enough from the substrate and Na^+ counterions (Fig. 2b). The slope of the electrostatic potential energy (V), dV/dz, where z is the surface

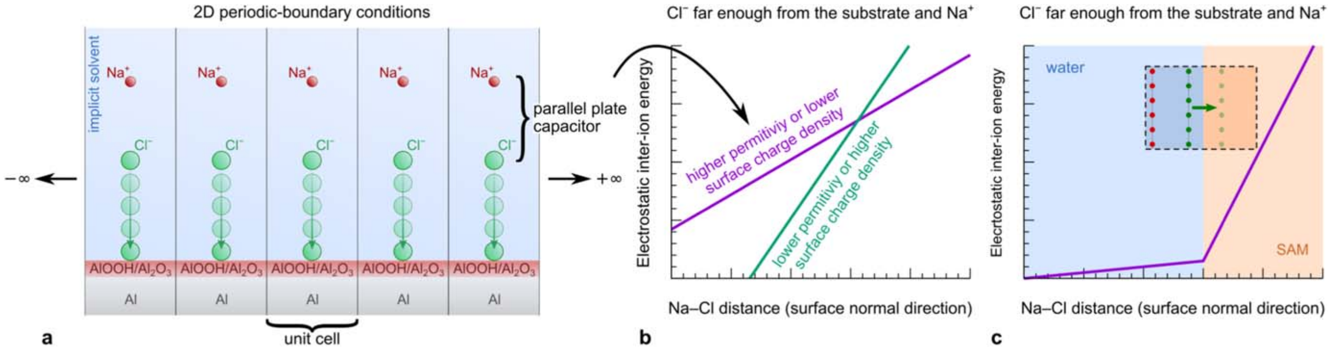

Figure 2. (a) Due to 2D periodic-boundary conditions, Cl^- ions and Na^+ counterions form two layers of charges reminiscent of a parallel plate capacitor. (b) The potential energy increases linearly with the increasing "vertical" distance between Na^+ and Cl^- (the slope increases with increasing the surface density of ions and decreases with increasing permittivity of the medium between the two layers). (c) Due to the high permittivity of water and low permittivity of the SAM, the potential energy increases considerably less in water than in the SAM.

normal direction, is proportional to:

$$\frac{dV}{dz} \propto \frac{q^2}{\varepsilon A} = \frac{q\sigma}{\varepsilon}, \qquad [1]$$

where q is the ion charge, ε the permittivity of the medium, A the supercell area, and σ the surface charge density, $\sigma = q/A$. The slope thus increases with increasing surface charge density and decreases with increasing permittivity. In water, the dV/dz slope is small due to the high permittivity of water. In contrast, the permittivity of the organic SAM was estimated[10] to be around 2.3,[a] implying a steep slope (Fig. 2c). Such slopes must be considered when interpreting the simulation results because they result from 2D PBC. In reality, Cl^- ions are more likely to penetrate SAM individually, that is, a given ion penetrates at a given time here and another ion at another time there. Interestingly, due to the superposition property of electrostatics, these slopes can be associated with an electrode potential, and the corresponding model was developed in the previous publication.[10]

Technical Details

Calculations were performed in the framework of DFT using the generalized gradient approximation (GGA) of Perdew-Burke-Ernzerhof (PBE)[12] with the periodic plane-wave code `VASP`.[13,14] We used projector-augmented-wave (PAW) potentials,[15,16] a plane-wave kinetic energy cutoff of 520 eV, and a Gaussian smearing of 0.1 eV. The semi-empirical dispersion correction of Grimme (DFT-D2)[17] was applied to account for dispersion interactions between organic molecules. The supercell that represents the substrate consists of a four-layer thick Al(111) slab covered by an ultra-thin oxide film (5 Å thick). The lateral dimensions of the supercell are mandated by the underlying Al(111) slab, where the calculated bulk lattice parameter of Al of 4.04 Å was used. Atomic positions were relaxed with the conjugate gradient algorithm until all force components were below 0.02 eV/Å.

The calculations were performed with an implicit water solvent using the `VASPsol` package,[18–20] modeled with a relative permittivity of 78.4.[21] The thickness of the implicit solvent region was set to more than 18 Å in the surface normal direction.

Model of the hydroxylated oxidized aluminum surface: AlOOH/Al_2O_3/Al(111).—The model of the hydroxylated oxide film on the aluminum surface was described in a previous publication.[1] It comprises a thin γ-Al_2O_3(111) film, hydroxylated at the surface and supported on Al(111). This model is herein designated as AlOOH/Al_2O_3/Al(111). It is built with an orthogonal $\begin{pmatrix} 3 & 0 \\ 2 & 4 \end{pmatrix}$ supercell of a 4-layer Al(111) slab that supports a 5 Å thick hydroxylated oxide film (Fig. 3). This orthogonal supercell is labeled as **S** in the following. Its lateral dimensions are $8.574 \times 9.901 \text{Å}^2 = 0.849 \text{ nm}^2$. A single Cl^- ion in the **S** supercell thus corresponds to the surface concentration of 1.18 Cl^-/nm^2. A four times smaller surface concentration of 0.29 Cl^-/nm^2 was also considered by using a (2 × 2)–**S** supercell, which corresponds to an orthogonal $\begin{pmatrix} 6 & 0 \\ 4 & 8 \end{pmatrix}$ supercell. The calculations with the **S** supercell were performed using a 3 × 3 × 1 Monkhorst–Pack k-point grid[22] and those with the (2 × 2)–**S** supercell using the Gamma k-point. The adsorbates, the thin oxide film, and the two uppermost metal layers at the oxide/metal interface were allowed to relax, whereas the bottom two layers of the Al(111) slab were fixed.

There are six hydroxylated surface Al ions in the **S** supercell. The stoichiometry of the outermost surface layer is $Al(OH)_2$, and it exhibits a hydroxyl density of 14.1 OH/nm^2, out of which 9.4 OH/nm^2 are in a bridging configuration (labeled as μ_2–OH), and 4.7 OH/nm^2 are in a monodentate configuration (μ_1–OH). Further details are given in Ref. 1.

The model for the study of Cl^- interaction with the bare AlOOH/Al_2O_3/Al(111) and SAM-covered surfaces.—To eliminate electrostatic long-range 3D PBC artifacts, mentioned in the introduction, we used a symmetric "double-sided" setup. The principle is shown in Fig. 4, where both pristine and SAM functionalized AlOOH/Al_2O_3/Al(111) substrates are considered in symmetric "double-sided" supercells (i.e. SAM/AlOOH/Al_2O_3/Al|Al\Al_2O_3\AlOOH\SAM), along with two implicitly solvated Cl^- ions (one below the substrate and the other above it). To maintain charge neutrality, a single Mg^{2+} ion per supercell is added into implicit water solvent; in the setup shown in Fig. 4, the substrate is located in the middle of the supercell along the surface normal direction, whereas Mg^{2+} is located at the bottom of the cell at $z = 0$ (this is why Mg^{2+} is shown with half-spheres at the bottom and top of the supercell). The position of Mg^{2+} is kept fixed, whereas the Cl^- ion is considered at different heights above the surface. This approach allows us to scrutinize the energetics of Cl^- insertion and adsorption in the presence and absence of the organic film. Only in the specific case where the Na^+/Cl^- ion-pair is considered, a "one-sided" slab is used because the ion-pair creates no dipole along the surface normal direction as it is oriented parallel to the surface.

Figure 4a schematically presents the approach and adsorption of Cl^- onto the pristine surface from implicit bulk water. Here, the initial state is the solvated Cl^-, and the final state is the chloride adsorbed on the AlOOH/Al_2O_3/Al(111) surface. In the final state, Cl^- is adsorbed on top of an OH group. In Fig. 4b, the AlOOH/Al_2O_3/Al(111) slab is functionalized with the SAM. For clarity, we use the following nomenclature: Cl^- is called "solvated" when it is far from the surface

---

[a] This value corresponds to the low-frequency experimental value of polyethylene[11] and the DFT-calculated optical dielectric constant of polyethylene.[10] The calculated optical dielectric constants of CA SAM layers range from 2.2 to 2.5, depending on the specifics of the rigid SAM model.[10] It should be noted that due to immobilized molecules in the SAM, the static and optical dielectric constants should be similar.

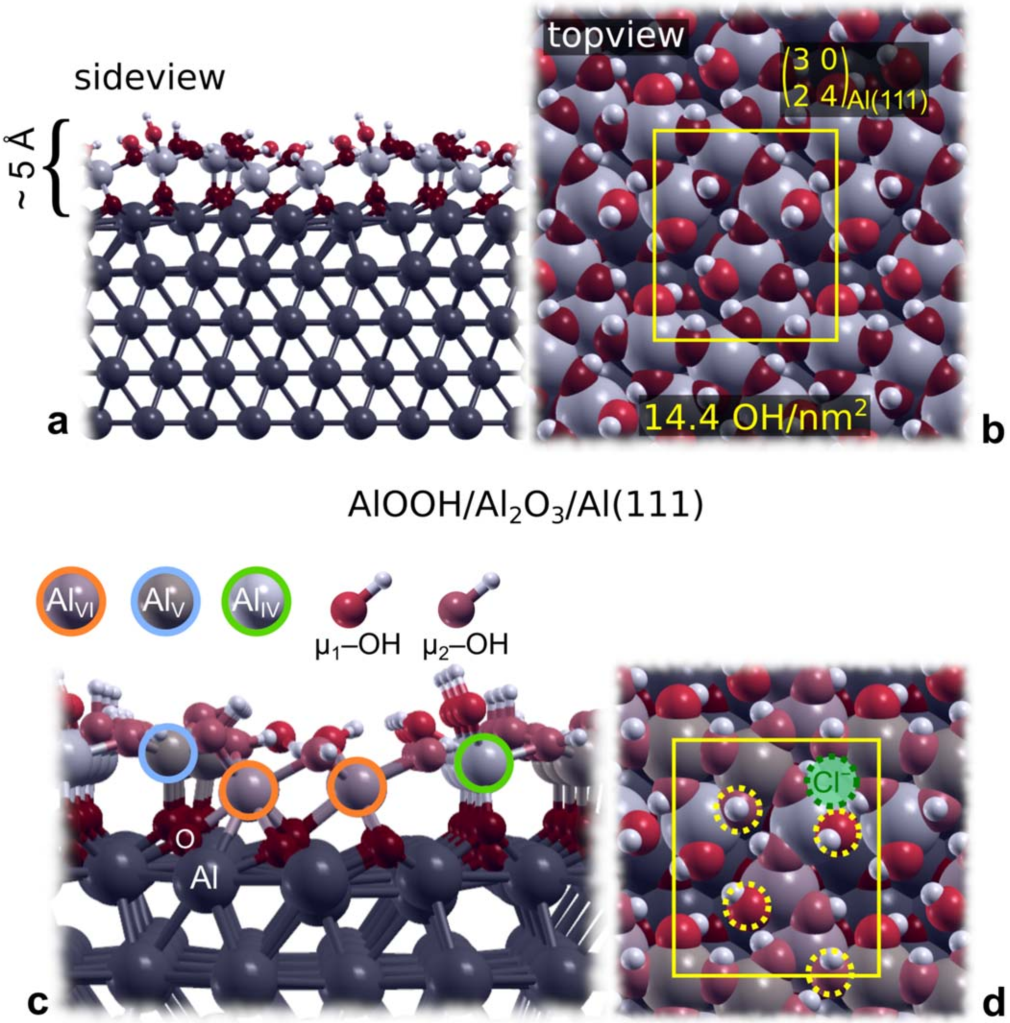

Figure 3. Model of the ultrathin hydroxylated oxide film above Al(111). (a) Side view and (b) top view with the $\mathbf{S} = \begin{pmatrix}3 & 0\\ 2 & 4\end{pmatrix}$ supercell shown by the yellow rectangle. (c,d) Side and top view with the indication of differently coordinated Al ions (Al$_{IV}$, Al$_V$, and Al$_{VI}$). On the top view in (d), the hydroxyl groups that are replaced by carboxylic groups are indicated by yellow dashed circles, whereas the Cl$^-$ adsorption site in the presence of SAM is indicated with a solid green circle. Note that atom sizes are drawn based on covalent radii, hence Al cations (gray) appear larger than O anions (red).

(either the oxide surface or the SAM surface, see Figs. 4a, 4b). This configuration gives the reference energy for solvated chloride (E_{IS}, where IS stands for the reference initial state configuration). All energy differences (ΔE) reported herein are measured with respect to E_{IS}, i.e.:

$$\Delta E = E - E_{IS}. \qquad [2]$$

The term "adsorbed" is used only when Cl$^-$ is adsorbed on the oxide surface. Otherwise, when the Cl$^-$ ion is in the SAM, we refer to "inserted" chloride. Two carboxylic acids were considered, one with 12 C atoms (CA-12) and the other with 6 C atoms (CA-6). The SAMs consisting of CA-6 and CA-12 molecules are named SAM-6 and SAM-12, respectively. For the SAM-12, two different SAM models were considered with differently tilted molecules.[5] In the first model, the molecules within the SAM point along the surface normal direction. This model, named upright-SAM-12, is hypothetical because the molecules within the SAM prefer to tilt to optimize the lateral intermolecular interactions. In the second model, the molecules are tilted about 40° from the surface normal direction. This model is labeled tilted-SAM-12.

The height of the Cl$^-$ ion (z_{Cl}) is measured with respect to the surface Al plane (z_{Al}), which corresponds to the average height of the Al ions in the topmost layer. The term "Al–Cl distance" thus corresponds to the vertical $|z_{Al} - z_{Cl}|$ distance.

Implicit-SAM models and other details.—Some calculations were also performed with semi-implicit models from the previous study,[10] where the Al substrate, the organic SAM film, and the aqueous solvent are implicitly described as dielectric continuum slabs, whereas Cl$^-$ ions and Na$^+$ counterions are treated explicitly by DFT using the PBE functional (here, two Na$^+$ ions are used in the "double-sided" setup instead of a single Mg^{2+} ion). The supercells used for these calculations were **S** and (2 × 2)–**S**. These calculations were performed with `Quantum ESPRESSO`[23,24] and the `Environ` plugin[25] using the soft-sphere-continuum-solvation (SoftCS) method.[26]

Molecular graphics were generated with `xcrysden`[27] and graph plotting was performed with the `Gnuplot` program.[28] Postprocessing of figures was done in `Inkscape`.[29]

Results

Cl$^-$ adsorption on AlOOH/Al$_2$O$_3$/Al(111).—We first consider the approach of the hydrated Cl$^-$ toward the pristine AlOOH/Al$_2$O$_3$/Al(111) surface and subsequent adsorption thereon. The calculations were performed with the symmetric double-sided **S** supercell, corresponding to the Cl$^-$ surface concentration of 1.18 Cl$^-$/nm^2. In the initial configuration, the Mg^{2+} and Cl$^-$ ions are located in the aqueous solution at 13.2 Å and 9.4 Å from the surface Al plane, respectively. During the simulation, the Mg^{2+} ion is kept

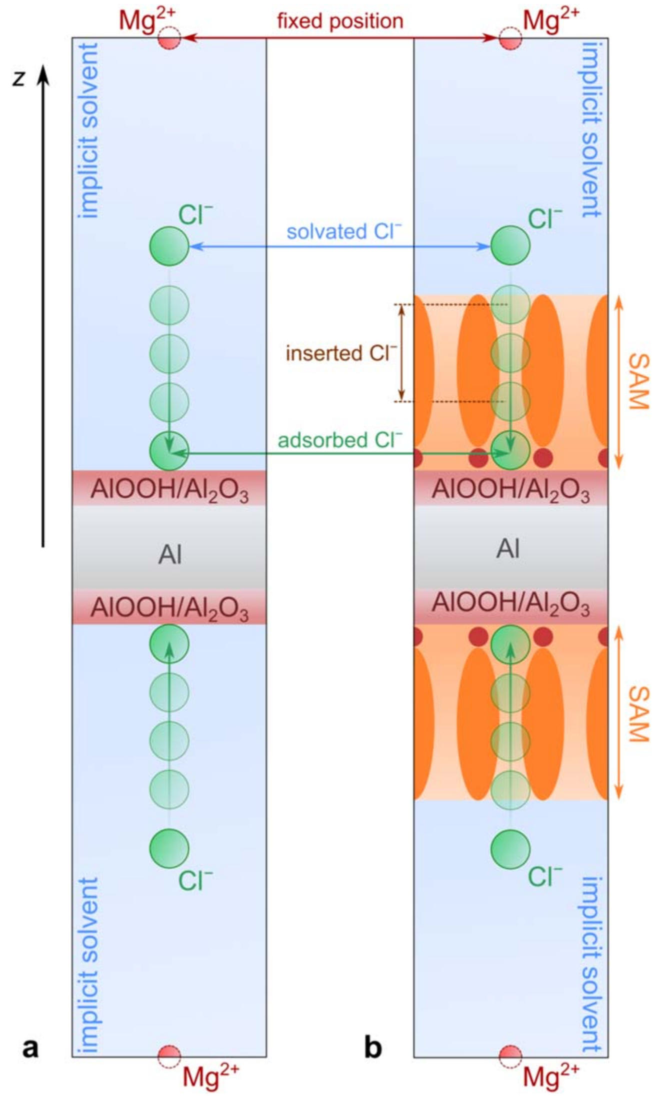

Figure 4. Scheme of the (a) pristine and (b) SAM-covered substrate in a "double-sided" symmetric setup. A Cl^- ion is added symmetrically above and below the Al substrate, and a single Mg^{2+} ion per supercell is used to maintain charge neutrality. This way, the dipole created by ions on one side of the substrate is canceled by the counter-dipole created on the other side of the substrate.

fixed, and Cl^- approaches the surface. The adsorption of Cl^- with Mg^{2+} in solution (the Mg–Cl vertical distance is 8.7 Å) is slightly exothermic, $\Delta E_{\rm DFT} = E_{\rm FS} - E_{\rm IS} = -0.19$ eV (Fig. 5), where $E_{\rm IS}$ and $E_{\rm FS}$ stand for the energies of the initial and final states. Notice that the energy rises when the Cl–Mg distance increases, as explained in the introduction.[10] Despite the high surface charge density of ions (Cl^- and Mg^{2+} ions in periodic cells can be seen as forming a parallel plate capacitor), the dE/dz slope is low due to the high water permittivity (charges are screened). The ΔE value extrapolated to zero surface concentration of Cl^- can be estimated as (in Hartree atomic units):

$$\Delta E_0 = \Delta E_{\rm DFT} + \frac{2\pi q^2 (z_{\rm FS} - z_{\rm IS})}{\varepsilon_{\rm water} A}, \qquad [3]$$

where $z_{\rm IS}$ and $z_{\rm FS}$ are the heights of Cl^- in the initial and final (adsorption) configurations, respectively (note that $z_{\rm FS} - z_{\rm IS} < 0$), $\varepsilon_{\rm water}$ is the relative permittivity of water, A is the supercell area (0.849 nm^2), and q is the charge of solvated ion ($q^2 = 1$). The so extrapolated ΔE_0 value is -0.26 eV; $\Delta E_{\rm DFT}$ and extrapolated ΔE_0 are also shown graphically in Fig. 5.

The second term on the right-hand side of Eq. 3 represents the electrostatic inter-ion contribution (cf. Fig. 2b) due to 2D PBC and is called the "electrostatic line" in Fig. 5. Notice that DFT calculated values closely follow it, provided that Cl^- is sufficiently away from the Al substrate ($\gtrsim$ 5.5 Å).

When the distance between Cl^- and the surface is short enough, lower than about 5 Å, the attractive interactions between Cl^- and the protons of OH groups (Fig. 5) result in H-bond formation, and attractive interactions begin to dominate. An H-bond between a surface proton and the chloride ion is formed, with an H–Cl distance of 2.1 Å (Fig. 5b). The chloride charge is -1 throughout the trajectory, except for the final configuration, where the Cl^- makes an H bond with the OH group. For this configuration, the Mg charge is unchanged (+2), but the Cl^- charge is -0.97, suggesting a weak charge transfer from Cl^- to H. Indeed, the proton charge of the interacting OH group is +0.61, to be compared with the average charge of +0.66 of the other surface protons.

Cl^- penetration into the SAM on $AlOOH/Al_2O_3/Al(111)$.—We now consider the Cl^- ingress into a SAM-12 on $AlOOH/Al_2O_3/Al(111)$. In our previous paper,[10] we modeled the SAMs with continuum dielectric slabs. This method allowed us to capture the electrostatic and solvation aspects of the interactions. Here, the semi-explicit DFT model allows us to also consider local inhomogeneities in the SAM and the steric effects of introducing ions in the SAM. The effect of local inhomogeneities in the SAM is addressed by considering two different SAM models, where the molecules either stand upright (the upright-SAM model) or are tilted (the tilted-SAM model). The two models differ in homogeneity: the upright-SAM model is inhomogeneous, consisting of clumped molecules and troughs (Fig. 7). This model is hypothetical because the molecules within the SAM prefer to tilt to optimize the lateral intermolecular interactions. It is used only as a simple model for discerning the effects of inhomogeneities in the SAM structure. In contrast, the tilted-SAM model is more homogeneous (Figs. 1 and 7), and due to molecular tilt, no solvent molecules are expected in the SAM. As for the estimation of steric effects, they need to be decoupled from the electrostatic effects, and to this end, we studied the ingress of the Xe atom, which has a similar size as Cl^- but is uncharged.

Steric hindrance effects: penetration of Xe atoms into the SAM.—The steric effects of introducing Cl^- ions into the SAM were estimated with the Xe atom, which has a similar size[b] as Cl^- but is uncharged and thus allows us to decouple steric effects from the long-range electrostatics effects. Figure 6 shows the Xe penetration profiles for the upright- and tilted-SAM-12 models at two different Xe surface concentrations, 1.18 Xe/nm^2 modeled by the **S** supercell and 0.29 Xe/nm^2 modeled by the (2 × 2)–**S** supercell. Here, the highest energy point before Xe hits the surface-repulsion wall is taken as the barrier; according to Fig. 6, Xe starts feeling the repulsion from the surface at Xe–Al distances lower than about 5 Å. For the upright-SAM-12, the calculated Xe penetration barrier is 0.26 eV at 1.18 Xe/nm^2 and 0.07 eV at 0.29 Xe/nm^2. In contrast, the tilted-SAM-12 is more homogeneous and denser with optimized lateral inter-chain interactions, hence it is not surprising that the Xe penetration barrier is higher (0.20 eV at 0.29 Xe/nm^2) than for the upright-SAM. The calculated barriers, therefore, imply that steric hindrance alone is insufficient for preventing the penetration of Cl^- toward the Al substrate because a barrier on the order of a few 0.1 eV can easily (rapidly) be overcome at room temperature.

Penetration of Cl^- ions into the SAM.—The penetration of Cl^- ions was investigated for the tilted-SAM and the hypothetical upright-SAM models at surface concentrations of 1.18 Cl^-/nm^2

---

[b] The covalent and van der Waals radii of Xe are estimated to 1.40 and 2.16 Å, respectively,[30,31] whereas the ionic radius of Cl^- is 1.81 Å.[32]

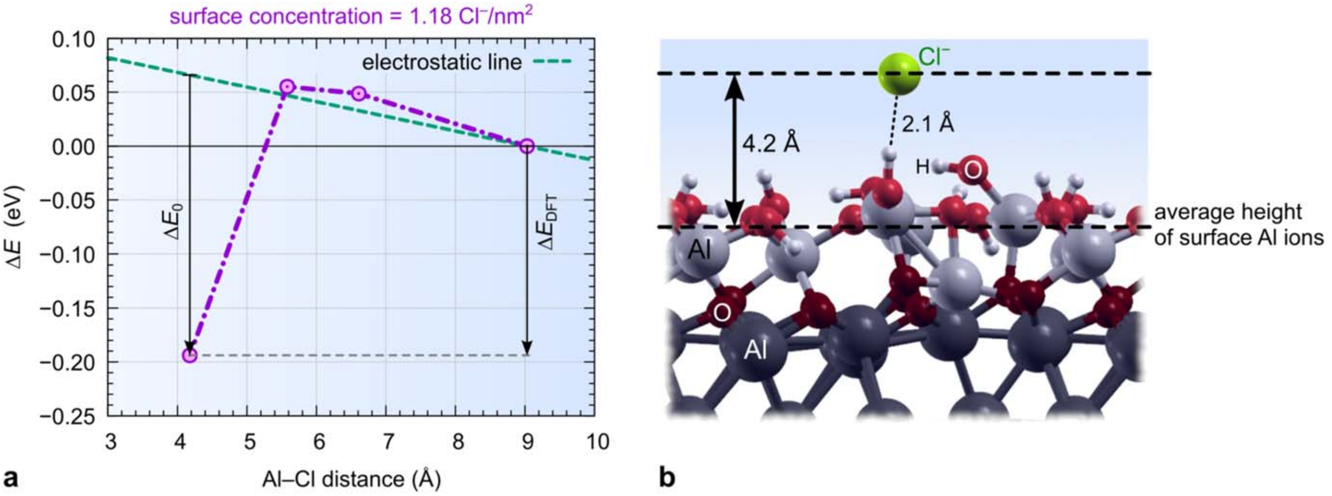

Figure 5. (a) Energy versus the Al–Cl distance for adsorption of Cl^- at bare $AlOOH/Al_2O_3/Al(111)$. The green dashed line shows the increase of electrostatic Na^+/Cl^- energy due to increasing distance between the Na^+ and Cl^- layers as Cl^- approaches the Al-substrate, corresponding to the second term on the right-hand side of Eq. 3. (b) A side-view snapshot of Cl-adsorption configuration (note that atom sizes are drawn based on covalent radii).

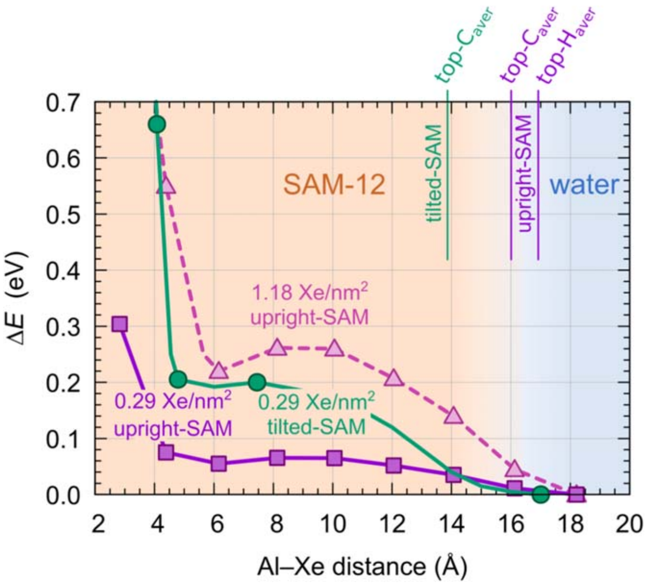

Figure 6. Energy penalty for penetration of Xe into SAM on Al substrate as calculated with the upright-SAM-12 model (purple) at the surface concentration of 1.18 and 0.29 Xe/nm^2 and the tilted-SAM-12 model (green) at 0.29 Xe/nm^2. The thickness of the SAM models is indicated by the average positions of topmost C atoms (top-C_{aver}) and topmost H atoms (top-H_{aver}).

(modeled by the double-sided **S** supercell) and 0.29 Cl^-/nm^2 (modeled by the double-sided (2 × 2)–**S** supercell). Top- and side-view snapshots of the relaxed upright- and tilted-SAM-12 models are shown in Fig. 7, whereas the calculated energy profiles for Cl^- penetration are compared to the results of the semi-implicit method[10] in Fig. 8. Due to arbitrariness in selecting the position of the water/SAM interface plane, it is not possible to univocally draw the electrostatic lines in Fig. 8. Hence, only the electrostatic slopes in the SAM at $\sigma = 1.18$ and 0.29 Cl^-/nm^2 are indicated instead, $dV/dz = 2\pi q\sigma/\varepsilon_{sam}$; the corresponding slope lines are plotted such that they align with the results of the implicit SAM models.

For the implicit-SAM of a thickness consistent with that of the upright-SAM-12, the semi-implicit model of the previous study[10] predicts the barriers of about 3 eV and 2.3 eV for Cl^- penetration at concentrations of 1.18 and 0.29 Cl^-/nm^2, respectively. In contrast, the current semi-explicit DFT model gives considerably smaller barriers of 1.83 eV and 0.68 eV for the upright-SAM-12 at 1.18 and 0.29 Cl^-/nm^2 (Fig. 8), respectively. The barrier for the tilted-SAM-12 at 0.29 Cl^-/nm^2 is much higher, about 2 eV, thus being much closer to the barrier predicted by the semi-implicit model in Ref. 10.

The results of Fig. 8 imply that the upright-SAM models give considerably smaller Cl^- penetration barriers than the tilted- and implicit-SAM models. This trend is further evidenced by Fig. 9, which compares the dependence of the Cl^- penetration barrier on the SAM thickness as given by the semi-implicit model[10] and the current semi-explicit DFT models; for the latter, both SAM-12 and SAM-6 are considered. The figure shows that the penetration barrier increases with the SAM thickness and, furthermore, that the barrier for the upright-SAM models is considerably smaller than that of the corresponding tilted- and implicit-SAM models. The reason is that due to non-optimal lateral distances between CA molecules in the upright-SAM, the molecules locally group, creating a non-uniform SAM structure with troughs between them (see Fig. 7). These troughs are large enough for the implicit solvent to enter them. Also, Cl^- ions penetrate the SAM along these troughs (note the Cl^- ions in the troughs in Fig. 7). The presence of the implicit solvent in troughs has two effects: it leads to more strongly solvated Cl^- and a better electrostatic screening between Cl^- ions.[c] Both effects lower the energy, leading to a much smaller Cl^- penetration barrier. Although the presence of implicit water in narrow troughs is likely an artifact (actual water molecules require large enough troughs to enter them), the current results provide a physical insight that is elaborated in the discussion Section and represents the basis for the new mechanism proposed therein. Furthermore, calculations reveal that when larger supercells are used, the CA molecules of the upright-SAM model tend to clump together due to lateral intermolecular interactions creating larger holes/troughs than those shown in Fig. 7; this aspect will be presented in more detail in a forthcoming publication. Hence, the possibility of water molecules entering the SAM is real enough to be considered seriously.

According to the electrostatic arguments, the Cl^- penetration barrier linearly increases with the SAM thickness (w_{sam}) and the Cl^- surface concentration (σ) because the inter-ion electrostatic contribution (ΔV) is proportional to (in Hartree atomic units):[10]

$$\Delta V = \left| \frac{2\pi q\sigma w_{sam}}{\varepsilon_{sam}} \right| . \quad [4]$$

[c] More strongly solvated Cl^- and a better electrostatic screening between Cl^- ions are related to the increased dielectric constant of the upright-SAM filled with the implicit water solvent in the troughs, resulting in a lower electrostatic slope of the upright-SAM-12 compared to that of the implicit-SAM model (Fig. 8).

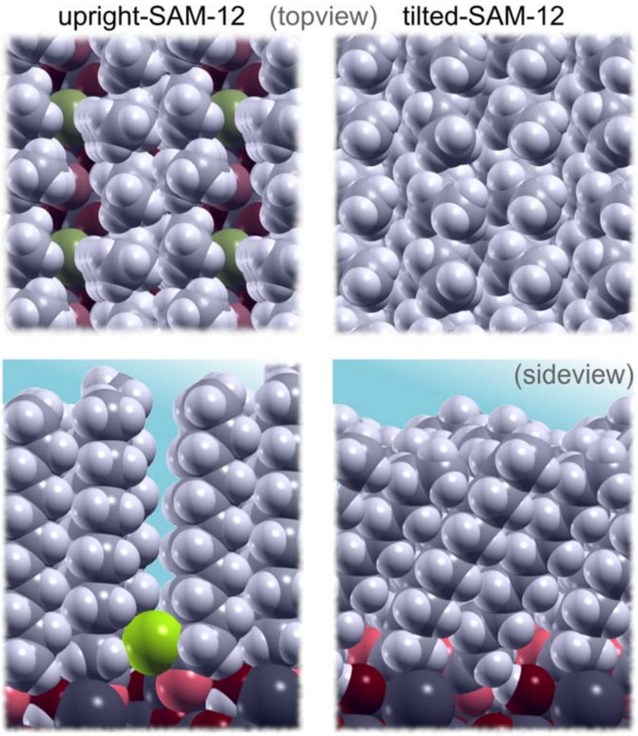

Figure 7. Top- and side-view snapshots of optimized upright-SAM-12 (left) and tilted-SAM-12 (right) on the Al substrate. Note that the CA molecules locally group in upright-SAM-12, creating troughs between them (note the Cl^- ions located in the bottom of troughs).

That the barrier increases with the SAM thickness is evidenced by Fig. 9. Furthermore, a linear dependence of Cl^- penetration barrier on the Cl^- surface concentration is confirmed by the semi-implicit calculations (Fig. 10). However, this linear dependence breaks down at too high concentrations, where it becomes energetically preferred for the Na^+/Cl^- double-layer to (partially) discharge. This is why the barrier at the high concentration of $\sigma = 1.18\ Cl^-/nm^2$ is smaller than four-times that of the four-times smaller concentration of 0.29 Cl^-/nm^2 (Figs. 8a), i.e. the respective barriers are 1.83 and 0.68 eV for upright-SAM-12 and 0.77 and 0.32 eV for upright-SAM-6 (Fig. 9).

According to the results of the implicit-SAM model,[10] the surface concentration of 1.18 Cl^-/nm^2 is so high that when Cl^- is deep enough into the SAM, the Cl^- ions deionize (i.e. the Na^+/Cl^- double-layer depolarizes) to reduce the electrostatic repulsion (cf. Fig. 9 of Ref. 10). The reason is that due to a low relative permittivity of SAM ($\varepsilon_{\text{sam}} = 2.3$), the dV/dz slope in the SAM is enormous, 0.46 eV/Å at 1.18 Cl^-/nm^2. Hence, by the electrostatic dV/dz effect alone, the energy rises by 4.6 eV when Cl^- enters 10 Å into the SAM at $\sigma = 1.18\ Cl^-/nm^2$. This value is slightly higher than the energy cost to completely discharge Na^+ in water and Cl^- in the SAM, estimated at about 4.3 eV.[d] Hence, when Cl^- is deeper than about 10 Å into the SAM, it is energetically more convenient for the Na^+/Cl^- double-layer to discharge.

Penetration of Na^+/Cl^- ion-pairs into the SAM.—In the previous publication,[10] we found that the penetration of Na^+/Cl^- ion-pairs into SAM is considerably inferior to that of Cl^- ions; the smallest identified Na^+/Cl^- ion-pair penetration barrier was about 2.2 eV. Current calculations with explicit-SAM models confirm this result. In particular, at Na^+/Cl^- concentration of 1.18 nm^{-2}, the Na^+/Cl^- ion-pair adsorption configuration is by about 2.1 eV less stable than the reference configuration with the Na^+/Cl^- in bulk aqueous solution.

Discussion

As anticipated in the introduction, current DFT calculations confirm that the barrier for the Cl^- penetration is considerably lower for the upright-SAM model than for the tilted-SAM model. The reason is that troughs (or holes) appear in the upright-SAM structure, and implicit solvent enters them, leading to more strongly solvated Cl^- ions and a better electrostatic screening between them. This effect is likely exaggerated because the implicit solvent enters the narrow slits more easily than the actual solvent consisting of explicit water molecules. Nevertheless, the possibility of solvent entering the SAM is sufficiently realistic to consider it seriously.

There are, therefore, two opposing effects: an "open" inhomogeneous SAM structure makes the penetration of Cl^- much easier for the just explained reasons, while lateral cohesive interactions prefer tilted alkyl chains and a homogeneously "closed" SAM structure. The question is, thus, which of the two effects wins, i.e. is it more convenient for Cl^- penetration (i) to locally open the SAM structure so that water fills the opening and Cl^- can penetrate dressed with its solvation shell,[e] or (ii) to penetrate directly into the homogeneous SAM as a naked Cl^-? These two different scenarios are schematically presented in Fig. 11.

The SAM deformation energy for making the space for the penetration of a naked Cl^- was estimated to be relatively low (cf. Fig. 6), but the deformation for creating a hole in the SAM that can accommodate Cl^- and water molecules is more substantial. A rough estimate of the corresponding energy cost can be obtained by considering the difference in stability between the tilted- and upright-SAM models. This energy difference was estimated in our

---

[d] The discharge energy can be estimated as $\Delta E_{\text{discharge}} = \text{EA(Cl)} - \text{IP(Na)} - \Delta G_{\text{solv}}(Na^+ \text{ in water}) - \Delta G_{\text{solv}}(Cl^- \text{ in SAM})$, where EA(Cl) and IP(Na) are the electron affinity of Cl and ionization potential of Na, and ΔG_{solv} represents the solvation free energy. The experimental values for EA(Cl), IP(Na), and $\Delta G_{\text{solv}}(Na^+ \text{ in water})$ are 3.62, 5.14 eV, and −4.28 eV, respectively. The calculated value of $\Delta G_{\text{solv}}(\text{Cl in SAM})$ is about −1.5 eV.[10] Here, the solvation contributions of neutral Na and Cl atoms were neglected because neutral species solvate weakly.

[e] In this case, the total penetration barrier can be estimated as the sum of the energy cost for opening the SAM and the penetration barrier in the "open" SAM.

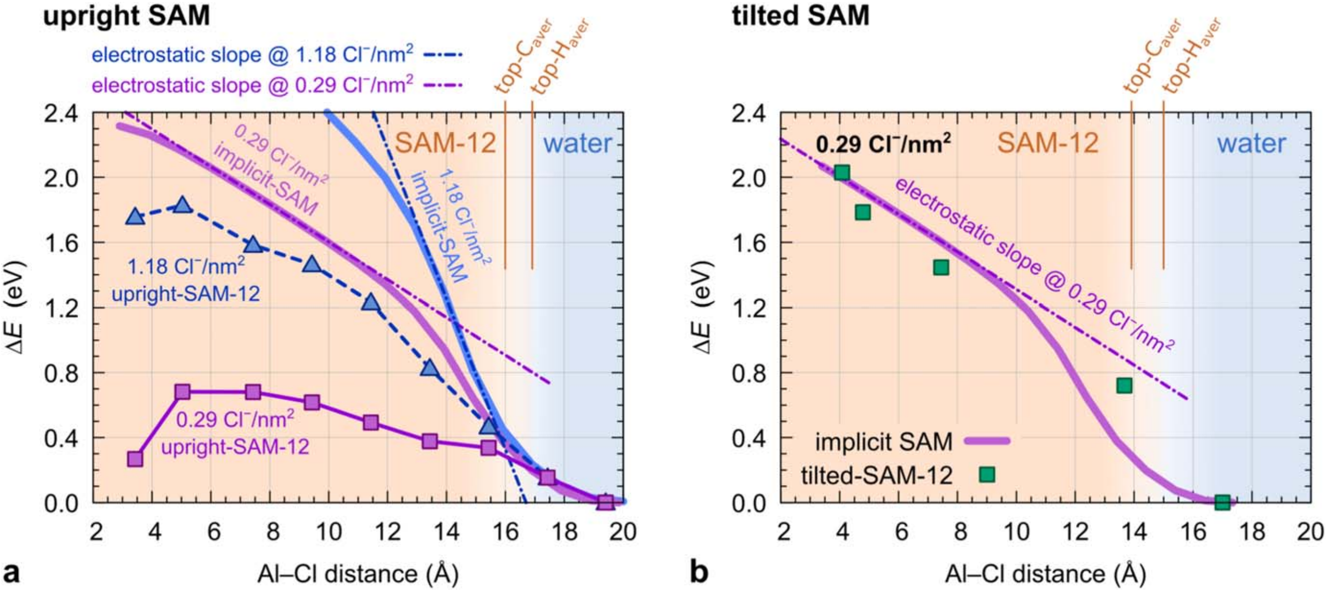

Figure 8. Energy penalty for the penetration of Cl^- into the SAM on the Al substrate as calculated with (a) the upright-SAM-12 model at the surface concentration of 1.18 $\mathrm{Cl}^-/\mathrm{nm}^2$ (blue) and 0.29 $\mathrm{Cl}^-/\mathrm{nm}^2$ (purple) and (b) the tilted-SAM-12 model at 0.29 $\mathrm{Cl}^-/\mathrm{nm}^2$ (green squares). The results of the corresponding implicit-SAM models are shown by thick pale curves in (a,b). Thin dash-dotted lines indicate the electrostatic slopes, Eq. 5, and are positioned to align with the results of the implicit SAM models.

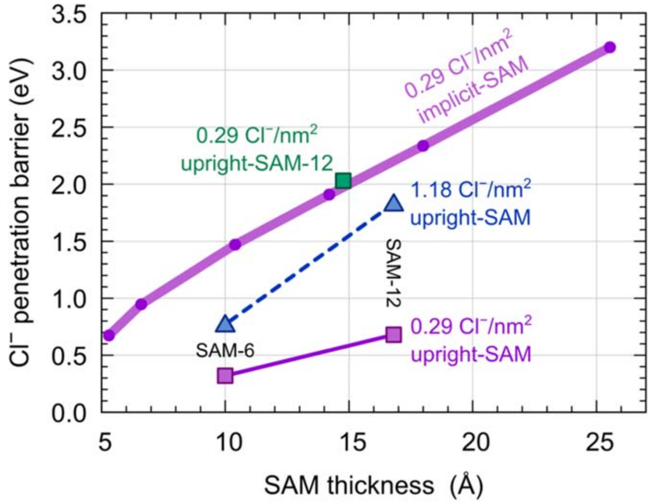

Figure 9. Cl^- penetration barriers versus SAM thickness for various SAM models at surface concentration of 1.18 $\mathrm{Cl}^-/\mathrm{nm}^2$ (blue) and 0.29 $\mathrm{Cl}^-/\mathrm{nm}^2$ (purple and green). SAM-6 and SAM-12 are considered for the explicit SAM models.

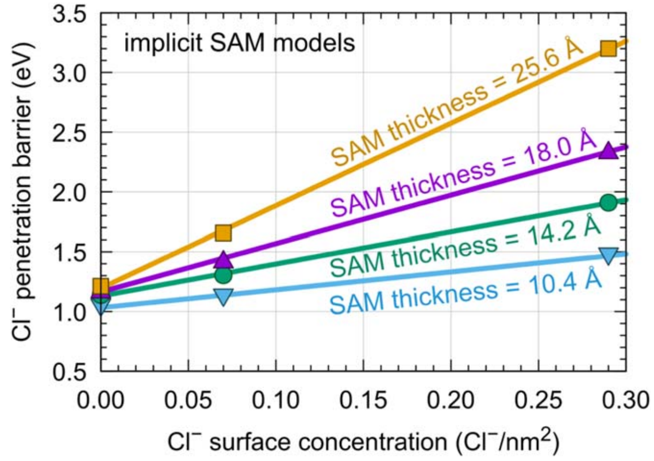

Figure 10. Cl^- penetration barriers versus Cl^- surface concentration as calculated with the implicit-SAM models of various thicknesses. The utilized thicknesses correspond approximately to the upright SAM-6, SAM-9, SAM-12, and SAM-18 models.

previous publication[5] to be about 0.2 eV/CA-molecule. At least four CA molecules need to space apart to create a local hole in the SAM structure, which should cost about $4 \times 0.2 = 0.8$ eV. This "opening" energy cost is smaller than the difference of 1.3 eV between the Cl^- penetration barrier in the tilted- and upright-SAM-12 models at 0.29 $\mathrm{Cl}^-/\mathrm{nm}^2$ (Fig. 8). At a lower surface concentration of Cl^-, this difference is smaller because, due to electrostatic reasons, the penetration barrier decreases with the surface concentration of Cl^- (Fig. 10). Yet, we can still assume that the penetration of Cl^- into SAM via local "opening" mechanism is viable. Furthermore, entropic effects tend to disorder the SAM structure, including molecular vacancies and regions with submaximal molecular coverage, thus facilitating the local SAM opening.

Irrespective of the SAM model (implicit or explicit), the calculations reveal that the barrier increases with the SAM thickness. One reason is due to inter-ion electrostatics (this contribution decreases with Cl^- surface concentration, see Fig. 10). The other reason is due to inferior Cl^- solvation in the SAM compared to that in the aqueous solvent (this difference was estimated to be about 1.4 eV).[10] Because the Cl^- ion is not a point object but has a finite size, this contribution increases with the SAM thickness up to about 10 Å and saturates afterward.[10]

In our previous publications,[6,7] we showed that only long-chain CAs are protective against Cl^- attack, whereas short-chain CAs did not exhibit a protective character. Based on our previous and present DFT calculations,[5,6,10] this observation can be explained as follows. First, due to molecular tilting, longer alkyl chains cover the Al surface more effectively. Furthermore, due to increased lateral cohesive forces, they also display a more exergonic adsorption free energy, resulting in a more stable and organized protective molecular film on the surface (indeed, it was experimentally observed[6] that only long-chain CAs fully cover the surface). Finally, longer alkyl chains lead to thicker SAMs which display higher Cl^- penetration barriers.

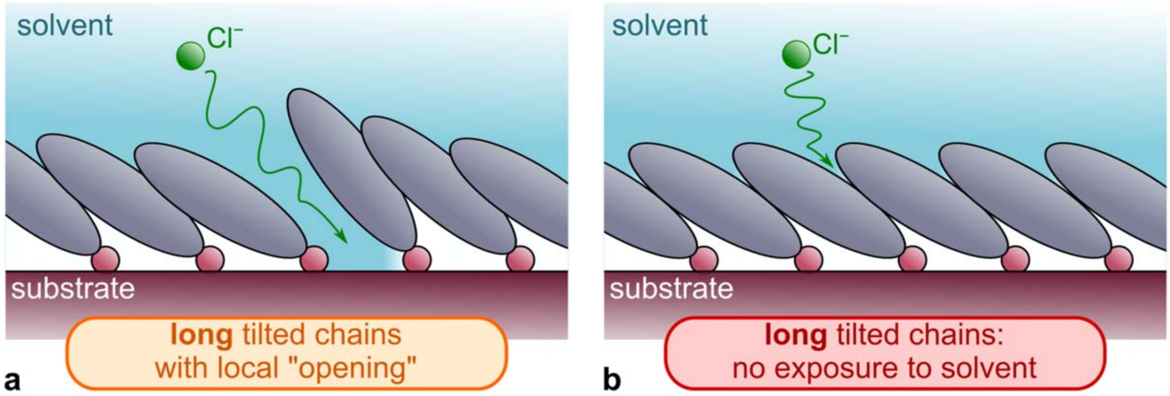

Figure 11. Two mechanisms of Cl^- penetrating the SAM: (a) the local "opening" mechanism, where the hole is created in the SAM that is large enough to accommodate water molecules and Cl^- with its water solvation shell, and (b) a naked Cl^- penetrating the homogeneous tilted-SAM model.

The increase of the penetration barrier with the SAM thickness due to inter-ion electrostatics can be seen as an artifact of 2D PBC (in reality, it is far more likely that a given ion penetrates at a given time here and another ion at another time there). However, this increase can be associated with the electrode potential, as shortly explained below (for more details, see Ref. 10). The 2D PBC electrostatic slope for moving the layer of Cl^- away from the layer of Na^+ is (in Hartree atomic units):

$$\frac{dV}{dz} = \frac{2\pi q\sigma}{\varepsilon_{sam}}, \quad [5]$$

where V stands for the inter-ion electrostatic energy. In contrast, the slope in the parallel plate capacitor or in the electrochemical Helmholtz double-layer for moving a charge inside a double-layer along the surface normal direction is:

$$\frac{dV_{DL}}{dz} = \frac{4\pi q\sigma}{\varepsilon_{sam}}, \quad [6]$$

where the subscript DL stands for double-layer and is used to distinguish V_{DL} from V. The dV_{DL}/dz slope is thus twice that of dV/dz in the 2D PBC simulation.[10] Let $E(z)$ be the Cl^- energy as a function of the Cl^- height z above the Al substrate. In the current 2D PBC simulations, $E(z)$ can be described as:[10]

$$E(z) = V(z) + \Delta\Delta G_{solv}(z) + O(z), \quad [7]$$

where $V(z)$ is the inter-ion electrostatic contribution, $\Delta\Delta G_{solv}(z)$ is the solvation contribution,[f] and all other effects are grouped into the $O(z)$ term (O stands for "other"). Note that in the limit of zero Cl^- concentration, the electrostatic $V(z)$ term vanishes, $V(z) \rightarrow 0$ (cf. Eqs. 4 and 5).

Now, let us consider that the electrode (i.e. Al substrate) is negatively charged with the surface charge density equivalent to that of Cl^- concentration in the 2D PBC simulation, and the positive counterions (in equivalent concentration) are located on top of the SAM. This way, an electrochemical Helmholtz double-layer is created, and the energy function for a single Cl^- ion (at the limit of zero Cl^- surface concentration) penetrating the SAM is:[10]

$$E_{DL}(z) = 2V(z) + \Delta\Delta G_{solv}(z) + O(z). \quad [8]$$

Note that the $O(z)$ term in this equation may differ from that in Eq. 7 due to different Cl^- concentrations in the two cases, but this term is not the focus here. Equation 8 implies that the contribution due to the double-layer electric field is twice that in the 2D PBC simulation. If the electrode is instead positively charged, the $E_{DL}(z)$ is given by:[10]

$$E_{DL}(z) = -2V(z) + \Delta\Delta G_{solv}(z) + O(z). \quad [9]$$

Equations 8 and 9 imply that Cl^- penetration barrier increases with potential cathodic to the potential of zero charge (PZC) and decreases with potential anodic to PZC, as one would intuitively expect. For further details, see Ref. 10.

Conclusions

The entry of Cl^- ions into carboxylate SAMs adsorbed on oxidized Al was investigated using DFT calculations, where Al substrate, SAM film, and ions are treated explicitly and only aqueous solvent implicitly. The explicit-SAM models allowed us to pinpoint further details of the mechanism by which Cl^- ions penetrate the SAM that the previous study[10] based on implicit-SAM models could not reveal. Hence, we scrutinized the effects of SAM deformation and inhomogeneities in the SAM structure on the Cl^- penetration barrier. We also confirmed the previous findings of the simplified implicit-SAM models that the Cl^- penetration barrier increases with the SAM thickness and with Cl^- concentration in the SAM and that Cl^- rather than the Na^+/Cl^- ion-pair diffuses into the organic layer.

We find that the deformation of the SAM during Cl^- penetration, though not negligible, does not significantly affect the penetration barrier. Hence, by steric hindrance alone, the SAM cannot effectively prevent the penetration of Cl^- toward the Al substrate because the barrier on the order of a few 0.1 eV can be overcome at room temperature. In contrast, inhomogeneities in the SAM structure have a much more considerable effect on the Cl^- penetration. In particular, the calculated Cl^- penetration barrier is considerably smaller in the hypothetical upright-SAM models, with the molecules pointing along the surface normal, than in the tilted-SAM models, where the molecules are significantly tilted. The structure of the tilted-SAM is considerably more homogeneous and denser than that of the upright-SAM, where large enough troughs (or holes) can form for water to enter them, leading to more strongly solvated Cl^- ions and a better electrostatic screening between them. Both effects lower the energy, resulting in a much smaller Cl^- penetration barrier. At the surface concentration of 0.29 Cl^-/nm^2, the calculated barriers for Cl^- penetration into the upright- and tilted-SAM-12 models are about 0.7 and 2 eV, respectively.

Although the presence of the implicit water solvent in narrow troughs of the currently utilized upright-SAM model is likely an artifact—actual water molecules require large enough troughs to enter them—the presented results provide the basis for the new mechanism proposed herein. In particular, the hypothetical upright-SAM structure is thermodynamically inferior to the tilted-SAM structure, but the Cl^- penetration barrier difference of 1.3 eV between the two SAM models is so remarkable that it suggests that instead of a naked Cl^- penetrating the dense and homogeneous tilted-SAM structure, it is more convenient to locally open the

---

[f] $\Delta\Delta G_{solv}$ is the difference in Cl^- solvation free energy in SAM and water, $\Delta\Delta G_{solv} = \Delta G_{solv}(Cl^- \text{ in SAM}) - \Delta G_{solv}(Cl^- \text{ in water})$.

homogeneous SAM structure by creating a hole that can accommodate water molecules so that Cl$^-$ dressed with its water solvation shell can penetrate it. The respective "opening" energy cost was currently estimated to be about 0.8 eV.

Acknowledgments

This work is a part of M-ERA.NET project entitled "COR_ID: Design of corrosion resistant coatings targeted for versatile applications". The financial support of the project by MESS (Ministry of Education, Science and Sport of Republic of Slovenia), Grant No. 3330-16-500040, and ANR (The French National Research Agency), Grant No. ANR-15-MERA-0004, is acknowledged. This work has been also supported by the Slovenian Research Agency (Grant No. P2-0393). DC and FC acknowledge GENCI for computational time on the French national supercomputer under the project DARI A 0060802217.

ORCID

Fatah Chiter https://orcid.org/0000-0002-1582-5318
Dominique Costa https://orcid.org/0000-0002-3781-9867
Matic Poberžnik https://orcid.org/0000-0002-4866-4346
Ingrid Milošev https://orcid.org/0000-0002-7633-9954
Philippe Marcus https://orcid.org/0000-0002-9140-0047
Anton Kokalj https://orcid.org/0000-0001-7237-0041

References

1. D. Costa, T. Ribeiro, F. Mercuri, G. Pacchioni, and P. Marcus, "Atomistic modeling of corrosion resistance: a first principles study of O_2 reduction on the Al(111) surface covered with a thin hydroxylated alumina film." *Adv. Mater. Interfaces*, **1**, 1300072 (2014).
2. D. Costa, T. Ribeiro, P. Cornette, and P. Marcus, "DFT modeling of corrosion inhibition by organic molecules: carboxylates as inhibitors of aluminum corrosion." *J. Phys. Chem. C*, **120**, 28607 (2016).
3. M. Poberžnik, D. Costa, A. Hemeryck, and A. Kokalj, "Insight into the bonding of silanols to oxidized aluminum surfaces." *J. Phys. Chem. C*, **122**, 9417 (2018).
4. M. Poberžnik and A. Kokalj, "Implausibility of bidentate bonding of the silanol headgroup to oxidized aluminum surfaces." *Appl. Surf. Sci.*, **492**, 909 (2019).
5. M. Poberžnik, F. Chiter, I. Milošev, P. Marcus, D. Costa, and A. Kokalj, "DFT study of n-alkyl carboxylic acids on oxidized aluminum surfaces: from standalone molecules to self-assembled-monolayers." *Appl. Surf. Sci.*, **525**, 146156 (2020).
6. I. Milošev et al., "Electrochemical, surface-analytical, and computational DFT study of alkaline etched aluminum modified by carboxylic acids for corrosion protection and hydrophobicity." *J. Electrochem. Soc.*, **166**, C3131 (2019).
7. I. Milošev et al., "Editors' choice—The effect of anchor group and alkyl backbone chain on performance of organic compounds as corrosion inhibitors for aluminum investigated using an integrative experimental-modeling approach." *J. Electrochem. Soc.*, **167**, 061509 (2020).
8. P. Marcus, V. Maurice, and H.-H. Strehblow, "Localized corrosion (pitting): A model of passivity breakdown including the role of the oxide layer nanostructure." *Corros. Sci.*, **50**, 2698 (2008).
9. P. M. Natishan and W. E. O'Grady, "Chloride ion interactions with oxide-covered aluminum leading to pitting corrosion: A review." *J. Electrochem. Soc.*, **161**, C421 (2014).
10. A. Kokalj and D. Costa, "Model study of penetration of Cl$^-$ ions from solution into organic self-assembled-monolayer on metal substrate: Trends and modeling aspects." *J. Electrochem. Soc.*, **168**, 071508 (2021).
11. D. R. Lide (ed.), *CRC Handbook of Chemistry and Physics* (CRC Press, Boca Raton, Florida USA) 85th ed. (2005).
12. J. P. Perdew, K. Burke, and M. Ernzerhof, "Generalized gradient approximation made simple." *Phys. Rev. Lett.*, **77**, 3865 (1996).
13. G. Kresse and J. Hafner, "Ab initio molecular-dynamics simulation of the liquid-metal-amorphous-semiconductor transition in germanium." *Phys. Rev. B*, **49**, 14251 (1994).
14. G. Kresse and J. Furthmüller, "Efficiency of ab-initio total energy calculations for metals and semiconductors using a plane-wave basis set." *Comput. Mater. Sci.*, **6**, 15 (1996).
15. P. E. Blöchl, "Projector augmented-wave method." *Phys. Rev. B*, **50**, 17953 (1994).
16. G. Kresse and D. Joubert, "From ultrasoft pseudopotentials to the projector augmented-wave method." *Phys. Rev. B*, **59**, 1758 (1999).
17. S. Grimme, "Semiempirical GGA-type density functional constructed with a long-range dispersion correction." *J. Comput. Chem.*, **27**, 1787 (2006).
18. K. Mathew, V. S. C. Kolluru, and R. G. Hennig, (2018), VASPsol: implicit solvation and electrolyte model for density-functional theory, https://github.com/henniggroup/VASPsol, doi: 10.5281/zenodo.2555053.
19. K. Mathew, R. Sundararaman, K. Letchworth-Weaver, T. A. Arias, and R. G. Hennig, "Implicit solvation model for density-functional study of nanocrystal surfaces and reaction pathways." *J. Chem. Phys.*, **140**, 084106 (2014).
20. K. Mathew, V. S. C. Kolluru, S. Mula, S. N. Steinmann, and R. G. Hennig, "Implicit self-consistent electrolyte model in plane-wave density-functional theory." *J. Chem. Phys.*, **151**, 234101 (2019).
21. D. P. Fernández, A. R. H. Goodwin, and J. M. H. L. Sengers, "Measurements of the relative permittivity of liquid water at frequencies in the range of 0.1 to 10 kHz and at temperatures between 273.1 and 373.2 K at ambient pressure." *Int. J. Thermophys.*, **16**, 929 (1995).
22. H. J. Monkhorst and J. D. Pack, "Special points for Brillouin-zone integrations." *Phys. Rev. B*, **13**, 5188 (1976).
23. P. Giannozzi et al., "Quantum ESPRESSO: a modular and open-source software project for quantum simulations of materials." *J. Phys: Condens. Matter*, **21**, 395502 (2009).
24. P. Giannozzi et al., "Advanced capabilities for materials modelling with Quantum ESPRESSO." *J. Phys: Condens. Matter*, **29**, 465901 (2017).
25. O. Andreussi, I. Dabo, and N. Marzari, "Revised self-consistent continuum solvation in electronic-structure calculations." *J. Phys. Chem.*, **136**, 064102 (2012).
26. G. Fisicaro, L. Genovese, O. Andreussi, S. Mandal, N. N. Nair, N. Marzari, and S. Goedecker, "Soft-sphere continuum solvation in electronic-structure calculations." *J. Chem. Theory Comput.*, **13**, 3829 (2017).
27. A. Kokalj, "XCrySDen–a new program for displaying crystalline structures and electron densities." *J. Mol. Graph. Model.*, **17**, 176 (1999).
28. T. Williams and C. Kelley et al., (2020), Gnuplot 5.4, http://gnuplot.info/.
29. Inkscape Project, Inkscape, version 1.0.2, (2021), https://inkscape.org.
30. B. Cordero, V. Gómez, A. E. Platero-Prats, M. Revés, J. Echeverría, E. Cremades, F. Barragán, and S. Alvarez, "Covalent radii revisited." *Dalton Trans.*, **2008**, 2832 (2008).
31. A. Bondi, "van der Waals volumes and radii." *J. Phys. Chem.*, **68**, 441 (1964).
32. R. D. Shannon, "Revised effective ionic radii and systematic studies of interatomic distances in halides and chalcogenides." *Acta Crystallogr. A*, **32**, 751 (1976).